Challenge Journal of Concrete Research Letters

Research Article

Axial compression behaviour of concrete-filled auxetic tubular short columns

Kemal Solak [a], Suleyman Nazif Orhan [a,*]

[a] *Department of Civil Engineering, Erzurum Technical University, 25050 Erzurum, Türkiye*

ABSTRACT

Concrete-filled steel columns (CFSCs) are of great interest in the literature as they are capable of carrying higher loads by combining the exceptional qualities of steel and concrete. With auxetic materials being introduced to civil engineering applications, the influence of these materials on CFSCs remains a matter of curiosity. The current study implements a nonlinear finite element analysis to evaluate the performance of circular CFSCs with six auxetic tubes under axial compression and the proposed numerical model was validated using published experimental data. The effect of the auxetic steel tube's porosity and Poisson's ratio on CFSCs was examined parametrically in terms of ultimate strength using the confined concrete model. Moreover, the stress distributions of the concrete and the auxetic steel tubes were also thoroughly examined. Based on the findings of the analysis, the ultimate load of CFSCs, utilising auxetic tubes with the same density and porosity but different Poisson's ratio, increased proportionally with the increase of auxetic behaviour. When it comes to auxetic tubes with different densities and porosities, the influence of the Poisson's ratio of the tubes diminished and the stiffness of tubes became more dominant over the mechanical characteristics of columns as the density of the auxetic steel tubes increased or decreased. The stiffness of the auxetic tubes reduced as porosity increased, as did the ultimate load of the columns. Additionally, the ultimate loads of the auxetic steel tube columns are found to be lower than those of bare steel tube columns filled with concrete due to perforations.

ARTICLE INFO

Article history:
Received 1 November 2022
Revised 27 November 2022
Accepted 20 December 2022

Keywords:
Concrete-filled steel columns
Auxetic tube
Confined concrete model
Axial load
Numerical analysis

1. Introduction

In modern structural industries, novel composites are continually being developed and investigated to enhance conventional structures' properties (Lacki et al. 2018; Gao et al. 2020). Steel-concrete composite columns are the most frequently encountered composite structures and many studies have previously demonstrated the benefits of employing steel-concrete composite columns in civil engineering (Soliman et al. 2013; Duarte et al. 2016). Concrete-filled steel composite columns are a type of steel-concrete composite and take advantage of concrete's excellent compression properties and steel's high tensile strength to exhibit superiority over conventional bare steel columns and reinforced concrete columns (Ellobody and Young 2011; Lacki et al. 2021). The confinement of the concrete core by a steel tube leads to a tri-axial state of compressive stresses, which improves the energy absorption, strength and ductility of the concrete. Moreover, the concrete infill prevents inward local buckling of the steel tube to a certain extent, thereby increasing the axial load capacity and buckling resistance of steel confined concrete columns (Hassanein et al. 2013; Gupta and Singh 2014; Ma et al. 2019). Even though many cross-sections of steel tubes can be used such as circular, elliptical, square, polygonal, and rectangular in concrete-filled steel columns, circular tubes provide the greatest confinement to the core of concrete by evenly dispersing stresses along the inward wall of the tube (Tao and Han 2006; Liang and Fragomeni 2009; Zha

* *Corresponding author*. Tel.: 444-5-388 ; Fax: +90-442-230-0036 ; E-mail address: s.orhan@erzurum.edu.tr (S. N. Orhan)
ISSN: 2548-0928 / DOI: https://doi.org/10.20528/cjcrl.2023.01.001

et al. 2013; Wang et al. 2022). The performance of circular concrete-filled steel columns (CFSC) under varied loading situations has been examined experimentally and numerically by researchers. Schneider (1998) conducted an experimental and analytical study to investigate the mechanical performance of compression loaded concrete-filled circular and rectangular steel tubes. The confinement of the concrete, as well as the effect of the steel tube cross section and the wall thickness of tubes on the ultimate strength were addressed in this study. Huang et al. (2002) studied the parametric analysis of concrete-filled columns with and without tie bars in terms of ultimate strength and ductility utilising circular and square cross-sections, both experimentally and numerically. Giakoumelis and Lam (2004) investigated high strength concrete-filled circular short columns under compression loading while revealing the effect of steel tube thickness, bond strength at the interface and confinement of the concrete core. They compared experimental values with different existing codes and suggested a coefficient to be used in codes to evaluate the influence of concrete confinement. Yu et al. (2008) attempted to investigate the feasibility of combining tubular steel columns with high strength concrete. In the experiments, specimens with varying cross-sections, slenderness ratios, and eccentricity loads were employed. As seen in the above studies, the steel tube's confinement effect has a major impact on the axial load capacity, which is mostly investigated (De Oliveira et al. 2010). Researchers investigated the confinement effect utilising spiral reinforcement (Kim et al. 2020) and steel rings (Lai and Ho 2014) due to the lack of perfect confinement of the bare steel tube.

Auxetic structures, which have a negative Poisson's ratio, are worth investigating with their exceptional features in various fields. Different geometric shapes and designs of auxetic structures have been offered in the literature to enhance their mechanical performance (Orhan and Erden 2022a, 2022b). One of the most common geometric shapes in auxetics is tubular structures. Because of their energy absorption capabilities, shear resistance, and bending resistance, auxetic tubulars are the most suitable structures for multidisciplinary studies. Ren et al. (2016) investigated the performance of buckling-induced auxetics experimentally and numerically in 3D tubular form under tension and compression states. Munib et al. (2015) fabricated a novel polymeric auxetic bone stent and investigated the mechanical character and deformation behaviour to assist alleviation of some of the current issues with bone internal fixation systems. Ren et al. (2022) experimentally examined the stiffness and energy absorption ability of foam-filled auxetic tubulars and compared results with finite element analysis. It has been observed that the interaction between the two materials is improved by transferring the axial load as lateral pressure to the inner wall of the tube. Solak and Orhan (2023) proposed a novel methodology to modify peanut-shaped auxetic tubular structures by rotating the unit cells by an angle and placing a stiffener at the exact centre of the peanut perforations. In this study, peanut-shaped tubular structures were numerically investigated and it was revealed that when stiffeners are used, high auxetic behaviour and high stiffness can coexist. Luo et al. (2022) utilised auxetic, non-auxetic, and bare steel tubes to generate concrete-filled composites. In this study, a new methodology was presented to improve the interface bonding between concrete and steel, local buckling of the steel tube and insufficient confinement of concrete.

Concrete-filled auxetic steel columns (CFASC) clearly appear to be leading a new trend in the literature. In the above study (Luo et al. 2022), it was demonstrated that employing the auxetic tube increased the confinement effect of concrete, and the findings were promising when compared to the non-auxetic encasement. The lack of studies in the literature on the mechanical behaviour of CFASCs with different Poisson's ratios and porosities has led to such a need. Therefore, in this study, it is aimed to adapt peanut-shaped perforated auxetic steel tubular structures to CFSCs to perform parametric analysis by using the finite element method. The mechanical character of the columns was examined under compression according to different parameters. Three distinct models with the same porosity, different negative Poisson's ratios and three models with different porosities were investigated and the findings were compared in terms of ultimate strength.

2. Materials and Method

2.1. Material properties of confined concrete

Since the column is loaded axially, the concrete infill expanded laterally and was restricted by the exterior steel tube. This confinement causes an increase in the strength and ductility of the concrete (Zhang et al. 2019), as shown in Fig. 1. Based on existing literature (Kedziora and Anwaar 2019), the constitutive stress-strain relationship and relevant parameters of confined concrete were derived by adapting the Drucker-Prager plasticity model.

For circular sections enclosed by steel tubes, Mander et al. (1988) proposed the following equation:

$$f'_{cc} = f'_{co} \cdot \left(-1.254 + 2.245 \cdot \left(\sqrt{\left(1 + 7.94 \cdot \frac{f_{rp}}{f'_{co}}\right)} - 2 \cdot \frac{f_{rp}}{f'_{co}} \right) \right) \quad (1)$$

where f'_{cc} is the compressive strength of confined concrete, f_{rp} is the confinement pressure and f'_{co} is the unconfined strength of concrete. The compressive strain in concrete ε_{co} can be determined using the information provided by Eurocode 2 (CEN, 2004) as follows:

$$\varepsilon_{co} = \begin{cases} 0.7 \cdot f_{cm}^{0.31} \rightarrow (0.7 \cdot f_{cm}^{0.31}) < 0.0028 \\ 0.0028 \rightarrow (0.7 \cdot f_{cm}^{0.31}) \geq 0.0028 \end{cases} \quad (2)$$

where f_{cm} is the mean value of the concrete cylinder compression strength. An empirical confinement pressure formula is provided as below using experimental findings by Hu et al. (2003):

$$f_{rp} = 0.3111 \cdot \left(\frac{D}{t} - 2\right)^{-1.027} \cdot f_y \quad (3)$$

where f_y is the yield strength of the steel tube, t is the thickness of the steel tube and D is the outer diameter of the tube. Based on the study of Xu et al. (2010), the ultimate residual compressive stress, f'_{cu}, can be calculated as follows:

$$f'_{cu} = \begin{cases} f'_{cc} \cdot \left(\frac{0.1 \cdot f_y}{f'_{co}}\right)^{0.1} \rightarrow \frac{D}{t} \leq 40 \\ f'_{cc} \cdot \left(\frac{0.1 \cdot f_y}{f'_{co}}\right)^{0.1} \cdot \left(\alpha + 1(1-\alpha) \cdot e^{\left(-\frac{D}{40.t}-1\right)}\right) \rightarrow \frac{D}{t} > 40 \end{cases} \quad (4)$$

where α is an empirical parameter. Based on the paper of Hu et al. (2005), the ultimate residual compressive strain ε_{cu} can be defined as follows:

$$\varepsilon_{cu} = 11 \cdot \varepsilon_{cc} \quad (5)$$

where ε_{cc} is the compressive strain in the confined concrete. The tensile strength f'_t of concrete can be expressed using the equation below:

$$f'_t = 0.56 \cdot (f'_{co})^{0.5} \quad (6)$$

Based on the study of Kupfer et al. (1969), the biaxial compressive strength f_{ccb} can be estimated as below:

$$f_{ccb} = 1.16 \cdot f'_{cc} \quad (7)$$

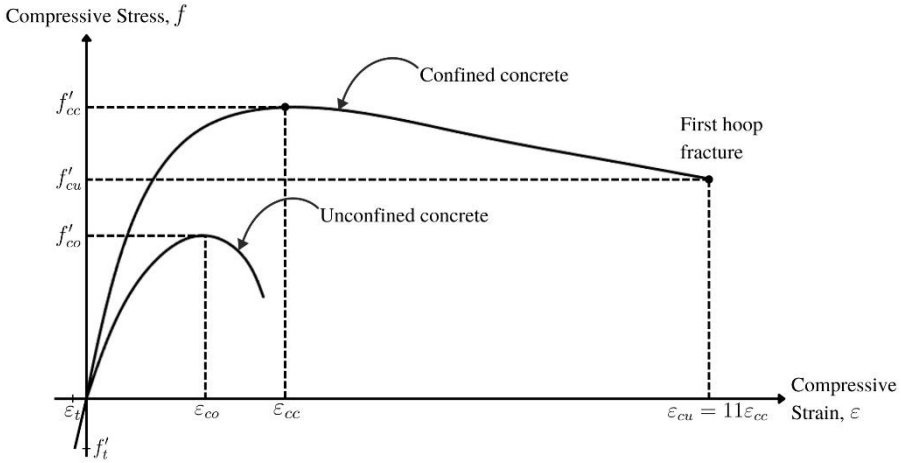

Fig. 1. Mander's stress-strain relation (1988) for both confined and unconfined concrete.

In this study, the uniaxial compressive strength, the biaxial compressive strength, and the uniaxial tensile strength values of Drucker-Prager and isotropic parameters of confined concrete were calculated using the above methodology and experimental data provided by Huang et al. (2002). Table 1 shows the concrete data utilised in the validation and parametric study, and these values are introduced to ANSYS for all models to perform nonlinear finite element simulation.

2.2. Design of the auxetic steel tubes and composite columns

When designing auxetic tubular structures, the form of the perforation is crucial since it affects the mechanical behaviour of the structure. Therefore Wang et al. (2020) presented a novel auxetic structure to minimise excessive stress concentration and provide improved auxetic behaviour. Peanut-shaped unit cells are employed to generate auxetic tubular structures and the geometric parameters of unit cells are shown in Fig. 2. Here, the small circle radius, the large circle radius, unit cell side length, distance between small circles and wall thickness of unit cell are represented as R_s, R_L, L, d and t, respectively.

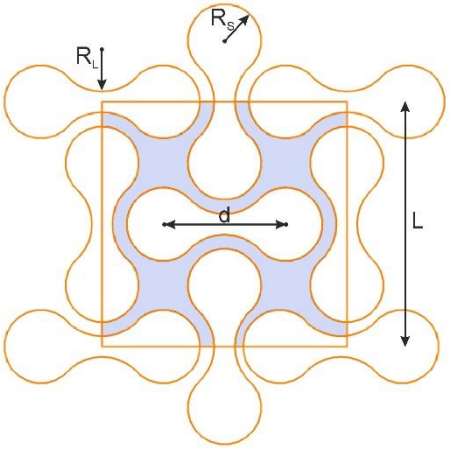

Fig. 2. Geometrical configuration of auxetic unit cell.

Table 1. Material properties of confined concrete.

Drucker-Prager plasticity parameters			Isotropic material parameters			
f'_{cc} (MPa)	f'_t (MPa)	f_{ccb} (MPa)	Unconfined compressive strength (MPa)	Modulus of elasticity (MPa)	Poisson's ratio	Density (kg/m^3)
33.68	2.92	39.07	27.15	24668	0.2	2400

Within the scope of this study, a total of six models were considered. Three have different unit cell lengths and the same porosity, while the other three have the same unit cell length and different porosity. In naming the models, auxetic steel tubes and composite columns were denoted by the letters T and C, respectively. The geometric details of unit cells used in steel tube modelling can be seen in Table 2.

Table 2. Dimensional properties of the unit cells used in auxetic steel tubes.

Tube name	R_s (mm)	R_L (mm)	L (mm)	d (mm)	t (mm)
A1T	9	12	60	30	5
A2T	7.5	10	50	25	5
A3T	4.5	6	30	15	5
B1T	4.5	6	30	15	5
B2T	3	4	30	10	5
B3T	2.5	5	30	8	5

All CFASCs are designed with a height of 300 mm, an outer diameter of 195.98 mm and a wall thickness of 5 mm by using SolidWorks software. All types of column are filled with concrete with a diameter of 185.98 mm and following the experimental study by Huang et al. (2002), CFSCs are clamped between two support plates, as seen in Fig. 3.

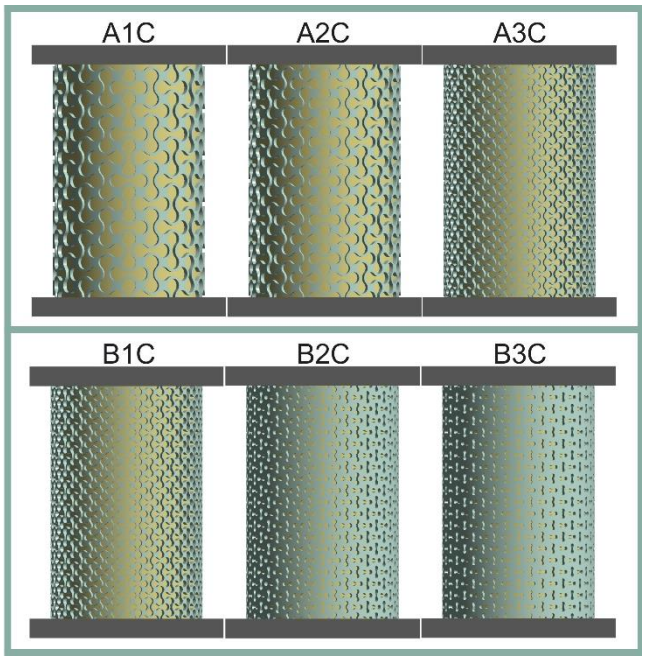

Fig. 3. Illustration of CFASC models.

The material properties of the steel tube enclosing the concrete were determined using the experimental data of the study of Huang et al. (2002), as seen in Table 3. Since the axially loaded concrete-filled steel tube was subject to high plastic deformation, isotropic hardening was also included in the analysis.

Table 3. Isotropic material properties of steel.

Yield strength (MPa)	Modulus of elasticity (GPa)	Poisson's ratio	Density (kg/m^3)
265.8	200	0.3	7850

2.3. Finite element simulation and verification

Numerical models of CFSCs were created using the Static Structural module of ANSYS 2022. In the analyses, eight-noded hexahedral elements with three translations of freedom at each node were employed for the concrete core and support plates, while four-noded tetrahedral elements were employed for all steel tubes due to the complex geometry of the auxetic steel tube. Based on several attempts to estimate an appropriate element size that provides a low computing time with relatively accurate results, the average mesh size was chosen as 10 mm for the concrete core and support plate and 2 mm for the auxetic steel tubes. The average "skewness" values of all components were also taken into account in the mesh study and kept constant between 0.2 and 0.3. Fig. 4 depicts the mesh discretisation of the finite elements used for CFASCs.

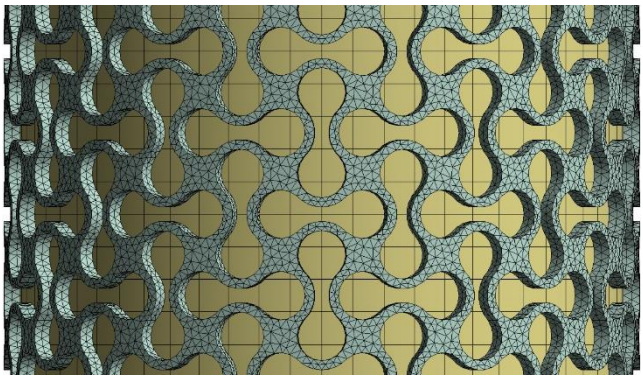

Fig. 4. Mesh discretisation of finite element model.

The interaction between concrete and steel was defined as frictional contact, and the coefficient of friction was determined as 0.6 in a direction tangent to the interaction face based on a study in the literature (Han et al. 2007). In addition, the bonded contact was employed to simulate a connection between the support plates and the steel tube. The axial load was gradually applied to the top plate, while the bottom plate was restricted for all rotations and translations. The main methodology of loading and boundary conditions is visualised in Fig. 5.

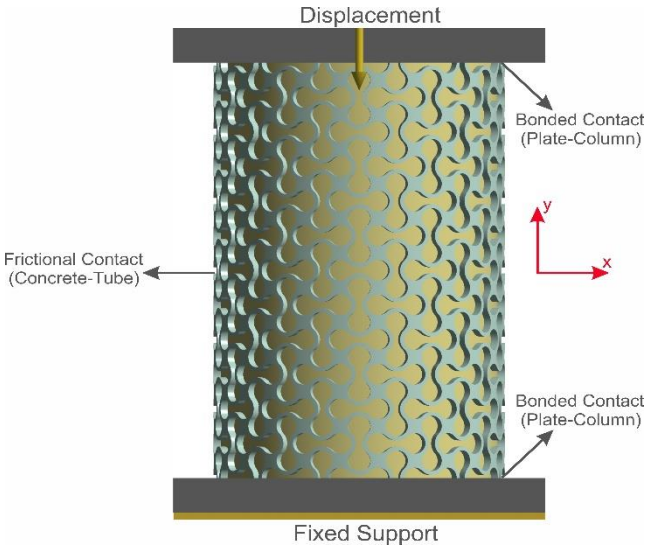

Fig. 5. Boundary and loading conditions of columns.

The mechanical characteristics of CFSC were compared with the experimental study of Huang et al. (2002) to confirm the accuracy and validity of the aforesaid numerical procedure. The CFSC used in the experiment has a height of 600 mm, an outer diameter of 200 mm and a steel tube wall thickness of 5 mm. For the finite element analysis of the validation model, the experiment's concrete and steel material properties and loading conditions were adopted by using abovementioned numerical method. At the end of the validation analysis, the load-deflection graph was produced, and ultimate compressive strength was calculated, and finally the findings were compared with the experimental results, as shown in Fig. 6. It can be seen that the load-deflection curve obtained from the finite element analysis and the curve acquired from the experiment are in agreement. While the ultimate compressive strength of the numerical analysis was 1953 kN, the ultimate compressive strength of the experiment was 2013 kN, with a relative error of 2.98%.

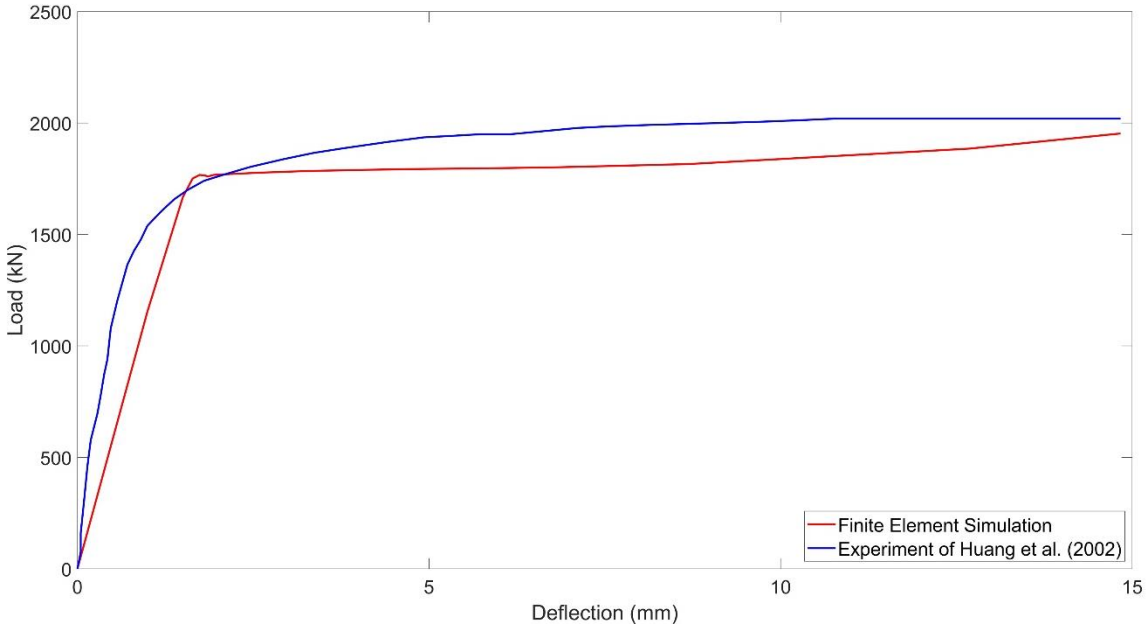

Fig. 6. Comparison of load-deflection relationships between FE simulation and experiment.

3. Results and Discussion

The ultimate load capacities of CFSCs modelled with different auxetic steel tubes were studied under axial compression. The Poisson's ratios and porosities of the auxetic tubes were determined as variable parameters and their effects on the mechanical behaviour of CFASCs were investigated. Firstly, models with different Poisson's ratios were designed without changing the porosity of the tubes to investigate only the direct effect of the Poisson's ratio on the mechanical behaviour of the columns. It was permitted to utilise different geometric parameters (R_s, R_L, L, d) to achieve the same porosity. The auxetic tubes with unit cell lengths of 30, 50 and 60 mm were created and the porosity of tubes was determined as 65.5%. Furthermore, The Poisson's ratios (ν_{xy}) were calculated using Equation 8 with the data taken from the outermost points of the centre of the models, as shown in Table 4. The A3T model, which has the largest unit cell, had the highest Poisson's ratio, while the A1T model had the lowest Poisson's ratio with the smallest unit cell. From these results, it can be seen that as the unit cell size increases, the Poisson's ratio decreases and these findings are compatible with the results of Zhang et al. (2021).

$$\nu_{xy} = -\frac{\text{lateral strain}}{\text{longitudinal strain}} = -\frac{\varepsilon_x}{\varepsilon_y} \tag{8}$$

Table 4. Poisson's ratio of auxetic steel tubes.

Tube name	L (mm)	Porosity	Poisson's ratio
A1T	60	0.655	-0.8308
A2T	50	0.655	-0.8492
A3T	30	0.655	-0.8601

Fig. 7 illustrates the load-deflection graph generated from the finite element analysis of models with identical material parameters, load-boundary conditions, and varying Poisson's ratios. The graph shows that there is a relation between the auxetic behaviour and the column's load carrying capacity. The greatest ultimate load of 1078.4 kN was achieved by the A3C model, while the lowest ultimate load of 1037.7 kN was obtained by the A1C model and the A2C model had a 1044.5 kN ultimate load. The conventional bare steel column has the same volume as the CFASC, however the bare steel column had a higher ultimate load of 1473.3 kN. As a result of their porous nature, auxetic steel tubes are inferior to bare steel.

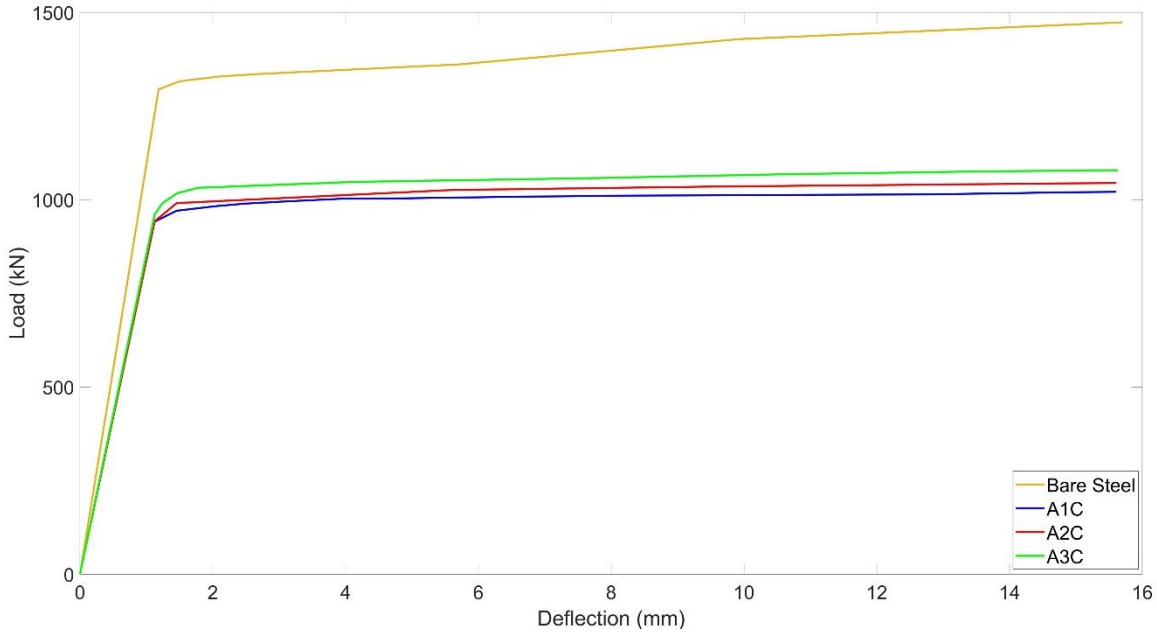

Fig. 7. Comparison of load-deflection relationships of A1C, A2C, A3C and bare steel models.

The A3C model exhibited the highest ultimate load among auxetic tubes with the same porosity, as shown in Fig. 7. Hence, further analyses were performed to thoroughly examine this structure. Therefore, the auxetic tube model with cell length L=30 mm was redesigned using different geometric parameters (R_s, R_L, d) without changing the unit cell length (L) with varied porosity, and their response to axial compression was examined. The Poisson's ratios were calculated using the approach described above. In addition, the auxetic structures' force-displacement curves were generated, and stiffness values were calculated using the slope of these curves due to changes in the porosity of the auxetic tubes. In Table 5, Poisson's ratios and stiffness values of auxetic steel tubes with different porosities are given. The highest porosity was seen in the B1T model, where the distance between the two circles was the greatest. As can be seen, as the distance (d) decreases, the space in the unit cell decreases and the structure has low porosity. Steel tubes with greater porosity exhibited more auxetic behaviour and lower stiffness values. The B3T model had the maximum stiffness value while exhibiting the least amount of auxetic behavior.

In Fig. 8, load-deflection curves of CFASC models with different tube porosity are shown. Here, although the B3C model showed the lowest auxetic behaviour, it had the highest ultimate load of 1630.7 kN. The B1C model with the highest auxetic behaviour had the lowest ultimate load of 1078.4 kN, while the B2C model had an ultimate load of 1516.9 kN. Furthermore, with increased porosity, the B3C model with a higher ultimate load than conventional bare steel was obtained. The graph shows that the influence of the Poisson's ratio on the ultimate load of models with varying porosity is nondominant. The ultimate load of the columns created by various porosities is dominated by the stiffness properties of the auxetic steel tubes. In short, whereas high porosity causes low stiffness and high auxetic behaviour, low stiffness is the primary factor in the decrease in ultimate load.

Table 5. Poisson's ratio and stiffness values of auxetic steel tubes.

Tube name	L (mm)	d (mm)	Porosity	Poisson's ratio	Stiffness (kN/mm)
B1T	30	15	0.655	-0.8601	8.6
B2T	30	10	0.293	-0.3215	427.5
B3T	30	8	0.216	-0.1021	802.2

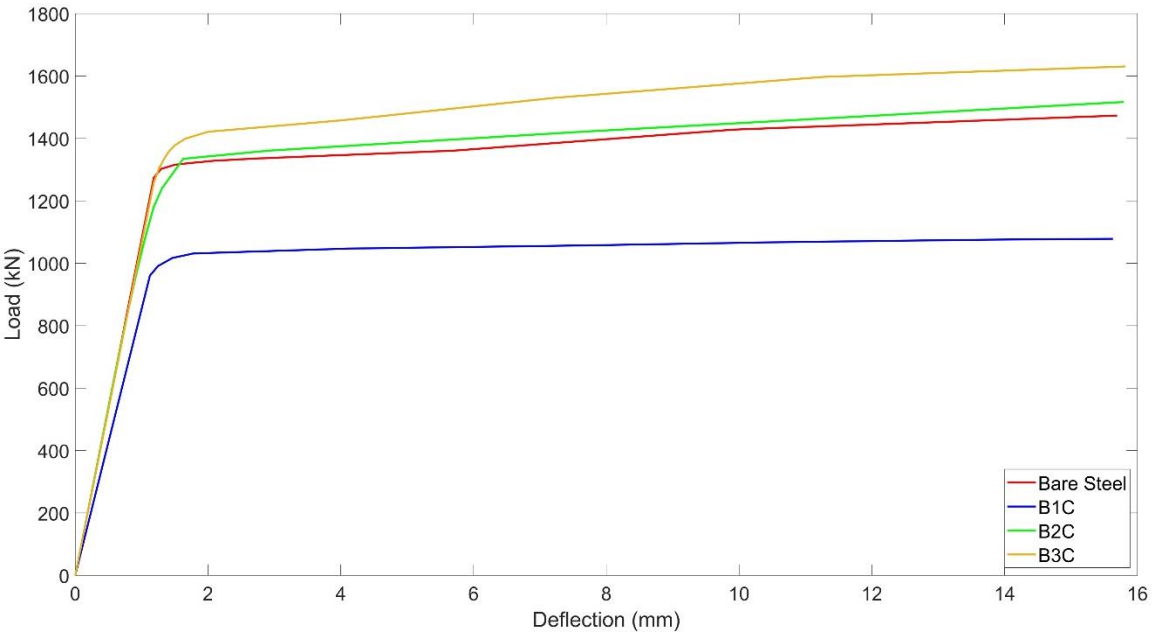

Fig. 8. Comparison of load-deflection relationships of B1C, B2C, B3C and bare steel models.

Within the scope of this research, the deformation modes and stress distributions of the structures were also studied. The maximum and average von Mises stress values of CFASCs under axial compression are given in Table 6, and the von Mises stress distributions are illustrated in Fig. 9. Since concrete has a positive Poisson's ratio, it tends to expand transversely under compression, and steel tubes with a negative Poisson's ratio counteract this to some extent. When loading was completed, the transverse expansion tendency of the concrete was dominant, causing transverse expansion in the auxetic steel tube. As a result of this expansion, high stresses were seen around the peanut perforations in all of the auxetic tubes with values between 367.34 MPa and 377 MPa. The average von Mises stresses at the concrete in all models were around 34 MPa. While the average von Mises stresses at the steel in the A1C, A2C, and A3C models were close to each other, this average stress value increased with porosity in the B1C, B2C and B3C models. Although B1C and bare steel had the same volume, the average von Mises stress of bare steel was higher.

Table 6. von Mises stresses of CFASCs.

von Mises Stress (MPa)		A1C	A2C	A3C	B1C	B2C	B3C	Bare Steel
Average	Concrete	34.2	34.3	34.4	34.4	34.4	34.6	34.9
	Steel tube	210.6	208.9	212.3	212.3	297.7	301.1	357.3
Maximum	Concrete	53.8	69.5	56.7	56.7	58.2	56.7	54.9
	Steel tube	377	368.7	367.3	367.3	376.5	376.6	377

4. Conclusions

In this study, the mechanical behaviour of concrete filled auxetic steel columns with a circular cross-section was investigated under the effect of axial compression. The finite element simulation was validated with the help of experimental results and the confirmed simulation was used to conduct a parametric study by using different geometric parameters of auxetic tubes. As a result of the parametric study, six distinct models were designed and examined, with the main parameters considering the Poisson's ratio and porosity of auxetic steel tubes. From the analyses, load-deflection curves and ultimate load capacities of all models were obtained. Moreover, the stress distributions of the concrete and the auxetic steel tubes were also thoroughly examined. A number of implications can be drawn from the findings of this study:

- The mechanical behaviour of concrete-filled auxetic steel columns can be estimated with the proposed finite element model with high accuracy and low time loss.
- Auxetic tubes with different Poisson's ratios and the same porosity have a significant effect on the ultimate load capacity of the columns as they encase the concrete core proportionally with the Poisson's ratios. Thence, steel tubes having a high auxetic tendency enhances the column's ultimate load.

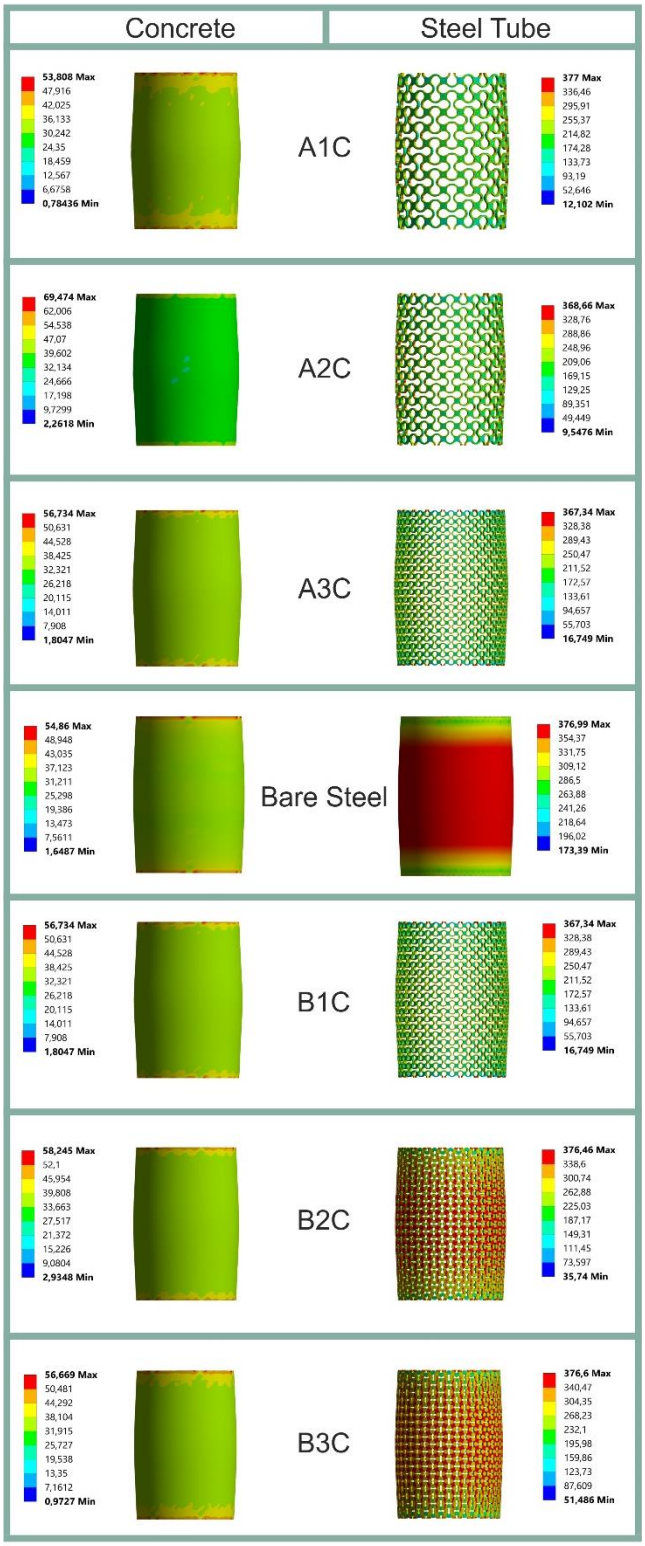

Fig. 9. Comparison of maximum von Mises stress distribution for all models.

- When porosity is considered as a variable parameter, the Poisson's ratio is no longer the determining factor, but instead stiffness is. When examining auxetic tubes with varying porosities, high porosity causes a low stiffness, which in turn decreases the ultimate load of the auxetic columns, while low porosity induces high stiffness and ultimate load.
- The ultimate loads of auxetic steel tube columns are lower than those of bare steel tube columns filled with concrete due to perforations. Nonetheless, further optimisation and parametric research can be conducted by developing new auxetic forms that yield superior outcomes to conventional concrete-filled columns.

Acknowledgements

None declared.

Funding

The authors received no financial support for the research, authorship, and/or publication of this manuscript.

Conflict of Interest

The authors declared no potential conflicts of interest with respect to the research, authorship, and/or publication of this manuscript.

References

CEN (2004). EN 1992-1-1: Eurocode 2: Design of concrete structures - Part 1-1: Buildings, rules and rules for buildings. BSI, London.

De Oliveira WLA, De Nardin S, De Cresce EALH, El Debs MK (2010). Evaluation of passive confinement in CFT columns. *Journal of Constructional Steel Research*, 66(4), 487-495.

Duarte APC, Silva BA, Silvestre N, De Brito J, Júlio E, Castro JM (2016). Finite element modelling of short steel tubes filled with rubberized concrete. *Composite Structures*, 150, 28-40.

Ellobody E, Young B (2011). Numerical simulation of concrete encased steel composite columns. *Journal of Constructional Steel Research*, 67(2), 211-222.

Gao S, Guo L, Zhang S, Peng Z (2020). Performance degradation of circular thin-walled CFST stub columns in high-latitude offshore region. *Thin-Walled Structures*, 154, 106906.

Giakoumelis G, Lam D (2004). Axial capacity of circular concrete-filled tube columns. *Journal of Constructional Steel Research*, 60(7), 1049-1068.

Gupta PK, Singh H (2014). Numerical study of confinement in short concrete filled steel tube columns. *Latin American Journal of Solids and Structures*, 11, 1445-1462.

Han LH, Yao GH, Tao Z (2007). Performance of concrete-filled thin-walled steel tubes under pure torsion. *Thin-Walled Structures*, 45(1), 24-36.

Hassanein MF, Kharoob OF, Liang QQ (2013). Behaviour of circular concrete-filled lean duplex stainless steel–carbon steel tubular short columns. *Engineering Structures*, 56, 83-94.

Hu HT, Huang CS, Wu MH, Wu YM (2003). Nonlinear analysis of axially loaded concrete-filled tube columns with confinement effect. *Journal of Structural Engineering-ASCE*, 129(10), 1322-1329.

Hu HT, Huang CS, Chen ZL (2005). Finite element analysis of CFT columns subjected to an axial compressive force and bending moment in combination. *Journal of Constructional Steel Research*, 61(12), 1692-1712.

Huang CS, Yeh YK, Liu GY, Hu HT, Tsai KC, Weng YT, Wang SH, Wu MH (2002). Axial load behavior of stiffened concrete-filled steel columns. *Journal of Structural Engineering-ASCE*, 128(9), 1222-1230.

Kedziora S, Anwaar MO (2019). Concrete-filled steel tubular (CFTS) columns subjected to eccentric compressive load. *Proceedings of the 15th Stability of Structures Symposium*, Zakopane, Poland.

Kim HG, Jeong CY, Kim DH, Kim KH (2020). Confinement effect of reinforced concrete columns with rectangular and octagon-shaped spirals. *Sustainability*, 12(19), 7981.

Kupfer H, Hilsdorf HK, Rusch H (1969). Behavior of concrete under biaxial stresses. *ACI Journal Proceedings*, 66(8), 656-666.

Lacki P, Derlatka A, Kasza P (2018). Comparison of steel-concrete composite column and steel column. *Composite Structures*, 202, 82-88.

Lacki P, Derlatka A, Kasza P, Gao S (2021). Numerical study of steel–concrete composite beam with composite dowels connectors. *Computers & Structures*, 255, 106618.

Lai MH, Ho JCM (2014). Behaviour of uni-axially loaded concrete-filled-steel-tube columns confined by external rings. *The Structural Design of Tall and Special Buildings*, 23(6), 403-426.

Liang QQ, Fragomeni S (2009). Nonlinear analysis of circular concrete-filled steel tubular short columns under axial loading. *Journal of Constructional Steel Research*, 65(12), 2186-2196.

Luo C, Ren X, Han D, Zhang XG, Zhong R, Zhang XY, Xie YM (2022). A novel concrete-filled auxetic tube composite structure: Design and compressive characteristic study. *Engineering Structures*, 268, 114759.

Ma H, Dong J, Hu G, Liu Y (2019). Axial compression performance of composite short columns composed of RAC-filled square steel tube and profile steel. *Journal of Constructional Steel Research*, 153, 416-430.

Mander JB, Priestley MJ, Park R (1988). Theoretical stress-strain model for confined concrete. *Journal of Structural Engineering*, 114(8), 1804-1826.

Munib Z, Ali MN, Ansari U, Mir M (2015). Auxetic polymeric bone stent for tubular fractures: design, fabrication and structural analysis. *Polymer-Plastics Technology and Engineering*, 54(16), 1667-1678.

Orhan SN, Erden Ş (2022a). Numerical investigation of the mechanical properties of 2D and 3D auxetic structures. *Smart Materials and Structures*, 31(6), 065011.

Orhan SN, Erden Ş (2022b). Design and finite element analysis of a novel auxetic structure. *Challenge Journal of Structural Mechanics*, 8(4), 159-165.

Ren X, Shen J, Ghaedizadeh A, Tian H, Xie YM (2016). A simple auxetic tubular structure with tunable mechanical properties. *Smart Materials and Structures*, 25(6), 065012.

Ren X, Zhang Y, Han CZ, Han D, Zhang XY, Zhang XG, Xie YM (2022). Mechanical properties of foam-filled auxetic circular tubes: Experimental and numerical study. *Thin-Walled Structures*, 170, 108584.

Schneider SP (1998). Axially loaded concrete-filled steel tubes. *Journal of Structural Engineering*, 124(10), 1125-1138.

Solak K, Orhan SN (2023). Performance evaluation of peanut-shaped tubular auxetics with enhanced stiffness: a finite element study. *Modelling and Simulation in Materials Science and Engineering*, 31(1), 015006.

Soliman KZ, Arafa AI, Elrakib TM (2013). Review of design codes of concrete encased steel short columns under axial compression. *HBRC Journal*, 9(2), 134-143.

Tao Z, Han LH (2006). Behaviour of concrete-filled double skin rectangular steel tubular beam–columns. *Journal of Constructional Steel Research*, 62(7), 631-646.

Wang H, Zhang Y, Lin W, Qin QH (2020). A novel two-dimensional mechanical metamaterial with negative Poisson's ratio. *Computational Materials Science*, 171, 109232.

Wang X, Fan F, Lai J (2022). Strength behavior of circular concrete-filled steel tube stub columns under axial compression: A review. *Construction and Building Materials*, 322, 126144.

Xu T, Xiang T, Zhao R, Zhan Y (2010). Nonlinear finite element analysis of circular concrete-filled steel tube structures. *Structural Engineering & Mechanics*, 35(3), 315.

Yu Q, Tao Z, Wu YX (2008). Experimental behaviour of high performance concrete-filled steel tubular columns. *Thin-Walled Structures*, 46(4), 362-370.

Zha X, Gong G, Liu X (2013). Study on behavior of concrete filled elliptical steel tube members part I: short and long columns under axial compression. *Advanced Steel Construction*, 9(2), 90-107.

Zhang Y, Wei Y, Bai J, Zhang Y (2019). Stress-strain model of an FRP-confined concrete filled steel tube under axial compression. *Thin-Walled Structures*, 142, 149-159.

Zhang C, Xiao SH, Qin QH, Wang H (2021). Tunable compressive properties of a novel auxetic tubular material with low stress level. *Thin-Walled Structures*, 164, 107882.